AIMS Mathematics, 8(8): 17650–17665.
DOI: 10.3934/math.2023901
Received: 27 March 2023
Revised: 03 May 2023
Accepted: 06 May 2023
Published: 23 May 2023

http://www.aimspress.com/journal/Math

Research article

Action minimizing orbits in the trapezoidal four body problem

Abdalla Mansur[1,2,*], Muhammad Shoaib[3], Iharka Szücs-Csillik[4], Daniel Offin[5] and Jack Brimberg[6]

[1] College of Science, Bani Waleed University, Bani Waleed, Libya

[2] Engineering and Information Technology Research Center, Bani Waleed, Libya

[3] Smart and Scientific Solutions, 32 Allerdyce Drive, Glasgow, G15 6RY, United Kingdom

[4] Romanian Academy, Astronomical Institute, Cluj-Napoca, Romania

[5] Queen's University, Mathematics and Statistics department, Kingston, Ontario, Canada

[6] The Royal Military College of Canada, Mathematics and Computer Science department, Kingston, Ontario, Canada

* **Correspondence:** Email: abmansur827@gmail.com, safridi@gmail.com.

Abstract: In this paper, we study the minimizing property for the isosceles trapezoid solutions of the four-body problem. We prove that the minimizers of the action functional restricted to homographic solutions are the Keplerian elliptical solutions, and this functional has a minimum equal to $\frac{3}{2}(2\pi)^{2/3}T^{1/3}\left(\frac{\xi(a,b)}{\eta(a,b)}\right)^{2/3}$. Further, we investigate the dynamical behavior in the trapezoidal four-body problem using the Poincaré surface of section method.

Keywords: central configuration; four-body problem; minimizers; trapezoidal problem; action functional; homographic solutions
Mathematics Subject Classification: 34C27, 34C35, 54H20

1. Introduction

For the planar four-body problem, let m_0, m_1, m_2, m_3 be four point masses moving in $\mathcal{R}^2$ in accordance with Newton's Law:

$$m_i\ddot{q}_i = \frac{\partial \mathcal{U}}{\partial q_i},$$

where $q_i \in \mathcal{R}^2$ denotes the position, and m_i the mass of the ith particle. With configuration $q = (q_0, q_1, q_2, q_3)$, the force function $\mathcal{U}(q)$ (negative of the potential energy) is defined as

$$\mathcal{U}(q) = \sum_{i<j} \frac{m_i m_j}{|q_i - q_j|}.$$

The Kinetic energy is defined as

$$\mathcal{K} = \sum_{i=0}^{3} \frac{m_i}{2} |\dot{q}_i|^2,$$

while the Hamiltonian governing the equations of motion is

$$\mathcal{H}(q, \dot{q}) = \mathcal{K}(\dot{q}) - \mathcal{U}(q), \quad \dot{q} = \frac{dq}{dt}.$$

For this problem, we define the action functional to be of the form:

$$\mathcal{A}(q) = \int_0^T \mathcal{L}(q, \dot{q}) dt,$$

where the Lagrangian $\mathcal{L}$ is defined as

$$\mathcal{L}(q, \dot{q}) = \sum_{i=0}^{3} \frac{m_i |\dot{q}_i|^2}{2} + \sum_{i<j} \frac{m_i m_j}{|q_i - q_j|}.$$

Due to the work of Sundman (1908) on the three-body problem, it is known that the action $\mathcal{A}_T$ stays finite along collision orbits of the equations of motion. For this reason, special care must be taken when considering the variational problem. If the action stays finite along a sequence of curves tending to collision, then such a limiting curve on the boundary of the functional space $\mathcal{A}_T$ could provide the minimizing loop. This is exactly the situation discovered by [1] for the Kepler problem.

Gordon [1] proved that the elliptic Keplerian orbit minimizes the Lagrangian action of the two body problem with periodic boundary conditions. He also found that the minimum value of the Keplerian action functional could be computed as

$$A^K = \int_0^T \frac{|\dot{q}|^2}{2} dt + \frac{\mu}{|q|} \geq \frac{3}{2} (\pi)^{2/3} (\mu)^{2/3} T^{1/3}. \tag{1.1}$$

In [2, 3], the authors have shown that the Lagrangian and Eulerian elliptical solutions for the planar three body problem are the variational minimizers of the Lagrangian action functional. It is also known that the homographic solutions to the rhombus four-body problem are the variational minimizers of the action functional restricted to rhombus loop spaces, [4–7]. Chen [8] studied the existence of a new family of periodic solutions for the planar four-body problem with equal masses. Chen minimized the solutions over one-quarter of the period $[0, T]$ using numerical integration. Abdallah et al. [4, 9] have extended Chen's solutions to include the minimization over the full period $[0, 4T]$ without involving the use of numerical techniques. Santoprete [10] uses a topological argument to show that there is at most one central configuration for each cyclic ordering of the masses. In this paper, we will show that the homographic solutions to the isosceles trapezoid four-body problem also minimize the action function, and the proof does not involve any numerical integration. This result can be useful in studying certain stability properties of the family of homographic solutions which belong to the isosceles trapezoid four-body problem.

2. Central configurations

An n-body system forms a planar non-collinear central configuration if

$$f_{ij} = \sum_{k=0,k\neq i,j}^{n-1} m_k(R_{ik} - R_{jk})\Delta_{ijk} = 0, \tag{2.1}$$

where $R_{ij} = r_{ij}^{-3}$ and $\Delta_{ijk} = (\boldsymbol{r}_i - \boldsymbol{r}_j) \wedge (\boldsymbol{r}_i - \boldsymbol{r}_k)$ represent the area of the triangle determined by the sides $\boldsymbol{r}_i - \boldsymbol{r}_j$ and $\boldsymbol{r}_i - \boldsymbol{r}_k$. Consider four positive point masses m_0, m_1, m_2 and m_3 having position vectors $\boldsymbol{r}_i$ and inter-body distances r_{ij}. For a general four-body setup, Eq (2.1) gives the following six central configuration equations when $n = 4$ [11–13]

$$\begin{aligned}
f_{01} &= m_2(R_{02} - R_{12})\Delta_{012} + m_3(R_{03} - R_{13})\Delta_{013} = 0,\\
f_{02} &= m_1(R_{01} - R_{21})\Delta_{021} + m_3(R_{03} - R_{23})\Delta_{023} = 0,\\
f_{03} &= m_1(R_{01} - R_{31})\Delta_{031} + m_2(R_{02} - R_{32})\Delta_{032} = 0,\\
f_{12} &= m_0(R_{10} - R_{20})\Delta_{120} + m_3(R_{13} - R_{23})\Delta_{123} = 0,\\
f_{13} &= m_0(R_{10} - R_{30})\Delta_{130} + m_2(R_{12} - R_{32})\Delta_{132} = 0,\\
f_{23} &= m_0(R_{20} - R_{30})\Delta_{230} + m_1(R_{21} - R_{31})\Delta_{231} = 0.
\end{aligned} \tag{2.2}$$

Consider four point masses $m_0 = m_1 = 1, m_2 = m_3$ on the vertices of a trapezoid. The four point masses have position coordinates $\mathbf{r}_0 = (-\frac{1}{2}, 0)$, $\mathbf{r}_1 = (\frac{1}{2}, 0)$, $\mathbf{r}_2 = (\frac{a}{2}, \sqrt{b^2 - (\frac{1-a}{2})^2})$, and $\mathbf{r}_3 = (-\frac{a}{2}, \sqrt{b^2 - (\frac{1-a}{2})^2})$ respectively. Using the definitions of R_{ij}, Δ_{ijk} and $\boldsymbol{r}_i$ $(i = 0, 1, 2, 3,)$, we obtain

$$R_{01} = 1, R_{02} = \frac{1}{\alpha} = R_{13}, R_{03} = \frac{1}{\beta} = R_{12}, R_{23} = \frac{1}{a^3},$$

$$\begin{aligned}
\Delta_{ijk} &= -\Delta_{jik} = -\Delta_{ikj} = -\Delta_{kji}, \Delta_{ijk} = \Delta_{jki} = \Delta_{kij},\\
\Delta_{ijk} &= 0,\ if\ i = j\ or\ i = k\ or\ j = k,\\
\Delta_{012} &= \gamma = \Delta_{013},\ \Delta_{023} = a\gamma = \Delta_{123},
\end{aligned} \tag{2.3}$$

where

$$\alpha = (a + b^2)^{3/2}, \beta = b^3, \gamma = \sqrt{b^2 - (\frac{1 - a}{2})^2}.$$

Using the specific values of R_{ij} and Δ_{ijk} from Eq (2.3), the central configuration equation (2.2) become

$$\begin{aligned}
f_{01} &= 0, f_{23} = 0,\\
f_{02} &= f_{13} = \gamma\left(-\frac{m_3}{a^2} + \frac{am_3}{\beta} + \frac{1}{\beta} - 1\right) = 0,\\
f_{03} &= f_{12} = \gamma\left(\frac{m_3}{a^2} - \frac{am_3}{\alpha} + \frac{1}{\alpha} - 1\right) = 0.
\end{aligned}$$

Solving $f_{02} = 0$ for m_3, we get

$$m_3 = m = \frac{a^2(\beta - 1)}{a^3 - \beta}. \tag{2.4}$$

Using the value of m from the above equation in $f_{03} = 0$, we obtain the following necessary and sufficient condition for the existence of Isosceles trapezoidal central configurations

$$C(a,b) = a^3(\alpha+\beta-2) - 2\alpha\beta + \alpha + \beta = 0.$$

The mass m_3 will be positive and unique in the region $R(a,b)$ given below.

$$\begin{aligned} R(a,b) &= \{(a,b)|(0<a<1 \wedge a<b<1) \\ &\vee \quad (a>1 \wedge 1<b<a)\}. \end{aligned} \tag{2.5}$$

The region $R(a,b)$ will form the region of central configurations for positive masses subject to the constraint $C(a,b) = 0$. The $R(a,b)$ and $C(a,b) = 0$ are given in Figure 1.

We use the numerical solution of $C(a,b) = 0$ and interpolation to write b as a function of a which will also allow us to write m as a function of only one variable.

$$b = f(a) = \begin{cases} f_1(a) \text{ when } a \in (0, 0.55) \\ f_2(a) \text{ when } a \in (0.55, 1), \end{cases}$$

where

$$\begin{aligned} f_1(a) &= 0.12a^3 + 0.06a^2 - 0.24a + 1, \\ f_2(a) &= 111.839a^6 - 502.035a^5 + 930.907a^4 - 912.067a^3 \\ &\quad +498.26a^2 - 144.032a + 18.1344. \end{aligned}$$

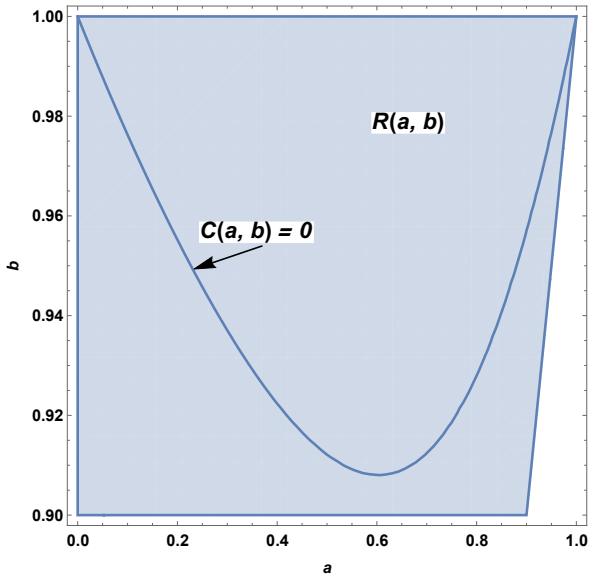

Figure 1. $R(a,b)$ and $C(a,b) = 0$.

3. Action minimizing orbits

In this section, we focus our attention on the homographic solutions $q_i(t) = \phi(t)q_{i,0}$ where $\phi : [0,T] \to \mathbb{C}^*$ is smooth, $\phi(0) = \phi(T)$ and $\deg(\phi) \neq 0$. We prove that these solutions are the variational minimizers of the action functional of the isosceles trapezoid four body problem.

The main result in this paper is the following theorem

Theorem 3.1. *The minimizers for $\mathcal{A}(q)$ restricted to the homographic solutions $q_i(t) = \phi(t)q_{i,0}$ are precisely the Keplerian elliptical solutions and the minimum of the action is equal to $\frac{3}{2}(2\pi)^{2/3}T^{1/3}\left(\frac{\xi(a,b)}{\eta(a,b)}\right)^{2/3}$.*

Let's call C_y the y -coordinate of the center of mass in the configuration analyzed in Section 2. Then

$$C_y := \frac{m\sqrt{4b^2 - 1 + 2a - a^2}}{2 + 2m}.$$

Performing a vertical translation of length C_y, we can arrive at a reference frame where the center of mass is located at $(0, 0)$, the bases are parallel to the x -axis, and the trapezoid has the y-axis as a symmetry axis. In this case, we have the following Cartesian coordinates for the points $q_{1,0}, q_{2,0}, q_{3,0}, q_{4,0}$:

$$q_{1,0} := (-\frac{1}{2}, -C_y), \quad q_{2,0} := (\frac{1}{2}, -C_y),$$
$$q_{3,0} := (\frac{a}{2}, h - C_y), \quad q_{4,0} := (-\frac{a}{2}, h - C_y).$$

Observe that $r_1 = |q_{1,0}| = |q_{2,0}| = \sqrt{\frac{1}{4} + C_y^2}$ and $r_3 := |q_{3,0}| = |q_{4,0}| = \sqrt{\frac{a^2}{4} + (h - C_y)^2}$. Moreover $|q_{1,0} - q_{2,0}| = 1$, $|q_{1,0} - q_{4,0}| = |q_{2,0} - q_{3,0}| = b$, $|q_{4,0} - q_{3,0}| = a$ and $|q_{4,0)} - q_{2,0}| = |q_{3,0} - q_{1,0}| = D := \sqrt{a + b^2}$, where D is the length of the diagonals of the trapezoid.

Proof. Recall that our solutions are homographic solutions and we want to restrict the action functional to this kind of solutions.

Let $|\dot{q}_1(t)|^2 = |\dot{\phi}(t)|^2 r_1^2$, then the kinetic energy term $\mathcal{K}$ is equal to

$$\begin{aligned}
\mathcal{K} &= \frac{1}{2}\sum_{i=0}^{3} m_i|\dot{q}_i(t)|^2 \\
&= |\dot{\phi}(t)|^2 r_1^2 + m r_3^2 |\dot{\phi}(t)|^2 \\
&= |\dot{\phi}(t)|^2 \left(r_1^2 + m r_3^2\right) \\
&= |\dot{q}_1(t)|^2 \left(1 + m\left(\frac{r_3}{r_1}\right)^2\right).
\end{aligned}$$

The potential is given by

$$\mathcal{U} = \sum_{0 \le i < j \le 3} \frac{m_i m_j}{|q_i - q_j|}.$$

Using $|q_i - q_j| = |\phi(t)||q_{i,0} - q_{j,0}|$ we get

$$\mathcal{U} = \frac{1}{|\phi(t)|}\left(1 + \frac{2m}{b} + \frac{m^2}{a} + \frac{2m}{D}\right).$$

Multiplying and dividing by r_1 we obtain

$$\mathcal{U} = \frac{1}{|q_1|}\left(r_1 + \frac{2mr_1}{b} + \frac{m^2 r_1}{a} + \frac{2mr_1}{D}\right).$$

The action restricted to this class of homographic solutions can be computed as below:

$$\begin{aligned}\mathcal{A} &= \int_0^T \left(1 + m\left(\frac{r_3}{r_1}\right)^2\right)|\dot{q}_1|^2 dt \\ &\quad + \int_0^T \left[r_1 + \frac{2mr_1}{b} + \frac{m^2 r_1}{a} + \frac{2mr_1}{D}\right]\frac{1}{|q_1|}dt \\ &= \left(2 + 2m\left(\frac{r_3}{r_1}\right)^2\right)\int_0^T \frac{|\dot{q}_1|^2}{2}dt \\ &\quad + \left[r_1 + \frac{2mr_1}{b} + \frac{m^2 r_1}{a} + \frac{2mr_1}{D}\right]\int_0^T \frac{1}{|q_1|}dt.\end{aligned}$$

Let

$$\eta(a,b) = \left(2 + 2m\left(\frac{r_3}{r_1}\right)^2\right),$$

and

$$\xi(a,b) = r_1 + \frac{2mr_1}{b} + \frac{m^2 r_1}{a} + \frac{2mr_1}{D}.$$

Then

$$\mathcal{A}(q) = \eta\int_0^T \frac{|\dot{q}_1|^2}{2}dt + \xi\int_0^T \frac{1}{|q_1|}dt.$$

The infimum of $\mathcal{A}(q)$ is

$$\begin{aligned}\inf_q \mathcal{A}(q) &= \inf_{(a,b)>0}\inf_{q_1}\left\{\eta\int_0^T \frac{|\dot{q}_1|^2}{2}dt + \xi\int_0^T \frac{1}{|q_1|}dt\right\} \\ &= \inf_{(a,b)>0}\left\{\eta\inf_{q_1}\left(\int_0^T \frac{|\dot{q}_1|^2}{2}dt + \frac{\xi}{\eta}\int_0^T \frac{1}{|q_1|}dt\right)\right\}.\end{aligned}$$

We use [1] to calculate the following infimum

$$\inf_{q_1}(\int_0^T \frac{|\dot{q}_1|^2}{2}dt + \frac{\xi}{\eta}\int_0^T \frac{1}{|q_1|}dt)\} = \frac{3}{2}(2\pi)^{\frac{2}{3}}T^{1/3}(\frac{\xi}{\eta})^{2/3}.$$

Then

$$\begin{aligned}\inf_q \mathcal{A}(q) &= \inf_{(a,b)>0}\left\{\eta(a,b)\frac{3}{2}(2\pi)^{2/3}T^{1/3}\left(\frac{\xi(a,b)}{\eta(a,b)}\right)^{2/3}\right\} \\ &= \inf_{(a,b)>0}\left\{\frac{3}{2}(2\pi)^{2/3}T^{1/3}\eta(a,b)^{1/3}\left(\xi(a,b)\right)^{2/3}\right\}.\end{aligned}$$

Let $\phi(a,b) = \frac{3}{2}(2\pi)^{2/3}T^{1/3}\eta(a,b)^{1/3}\xi(a,b)^{2/3}$.The function $\phi(a,b)$ attains its infimum at (a_0,b_0) if and only if $\eta(a,b)\xi(a,b)^2$ attains its infimum at (a_0,b_0).

Taking advantage of the approximation obtained for b from $C(a,b) = 0$, we write $\phi(a,b)$ as a function of a only:

$$\phi(a) = \frac{3}{2}(2\pi)^{2/3}T^{1/3}\eta(a)^{1/3}\xi(a)^{2/3},$$

where

$$\eta(a) = \left(\frac{a^2}{4} + \left(\sqrt{f(a)^2 - \frac{1}{4}(a-1)^2} - g(a)\right)^2\right) \cdot$$
$$\cdot 2a^2\left(1 - f(a)^3\right) / \left[\left(f(a)^3 - a^3\right)\left(g(a)^2 + \frac{1}{4}\right)\right] + 2,$$

$$f(a) = b,$$

$$g(a) = \frac{a^2\sqrt{4f(a)^2 - (a-1)^2}\left(f(a)^3 - 1\right)}{2\left(\left(a^2-1\right)f(a)^3 + (a-1)a^2\right)}.$$

To show that $\phi(a)$ is convex we need to show that $\frac{d^2\phi(a)}{da^2} > 0$. For this purpose we rewrite $\phi(a)$ as $\phi(a) = \eta(a)\xi(a)^2$.

$$\begin{aligned}\frac{d^2\phi(a)}{da^2} &= \xi(a)^2\eta''(a) + 4\xi(a)\eta'(a)\xi'(a) \\ &\quad +2\eta(a)\xi(a)\xi''(a) + 2\eta(a)\xi'^2,\end{aligned}$$

where $\eta'(a)$, $\eta''(a)$, $\xi'(a)$ and $\xi''(a)$ are given in the appendix. To show that $\phi''(a) > 0$, we first check the sign of each of the functions involved. Since $a > 0$, $f(a)^3 - a^3 > 0$, $1 - f(a)^3 > 0$, therefore $\eta(a) > 0$. Similarly, $\xi(a)$ can be shown to be positive for all $a \in (0, 1)$. The derivatives of $\eta(a)$ and $\xi(a)$ are given in Figures 2 and 3. It is clear from the graphs that $\eta'(a), \xi'(a)$, and $\xi''(a)$ are positive when $a \in (0, 0.92)$. The second derivative of $\eta(a)$ is negative when $a > 0.67$; however it doesn't effect the positivity of $\phi''(a)$ since the remaining terms dominate the term which has $\eta''(a)$. This can be confirmed by the graph of $\phi''(a)$ given in Figure 4. This proves that the function $\phi(a)$ is convex when $a \in (0, 0.92)$.

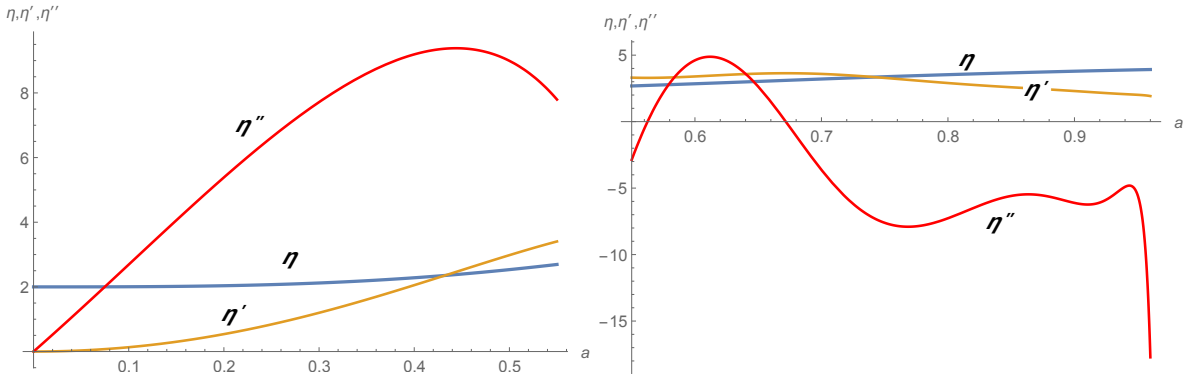

Figure 2. $\eta(a), \eta'(a)$ and $\eta''(a)$.

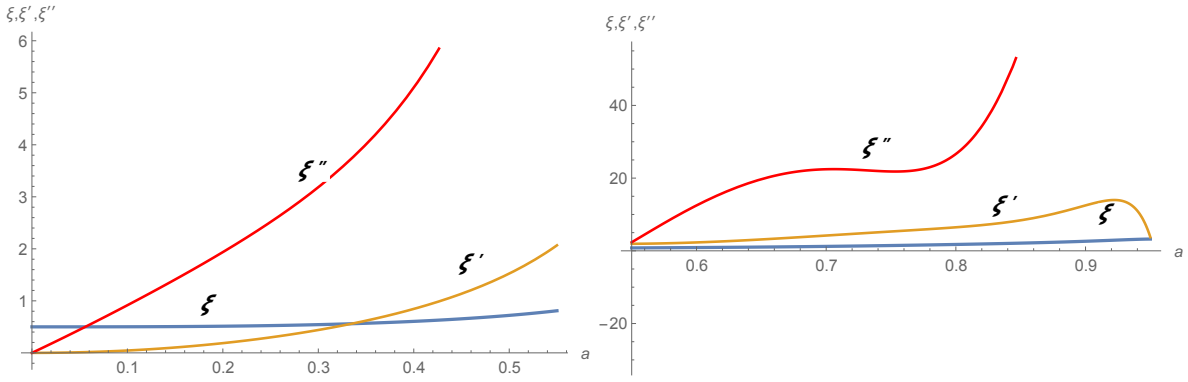

Figure 3. $\xi(a), \xi'(a)$ and $\xi''(a)$.

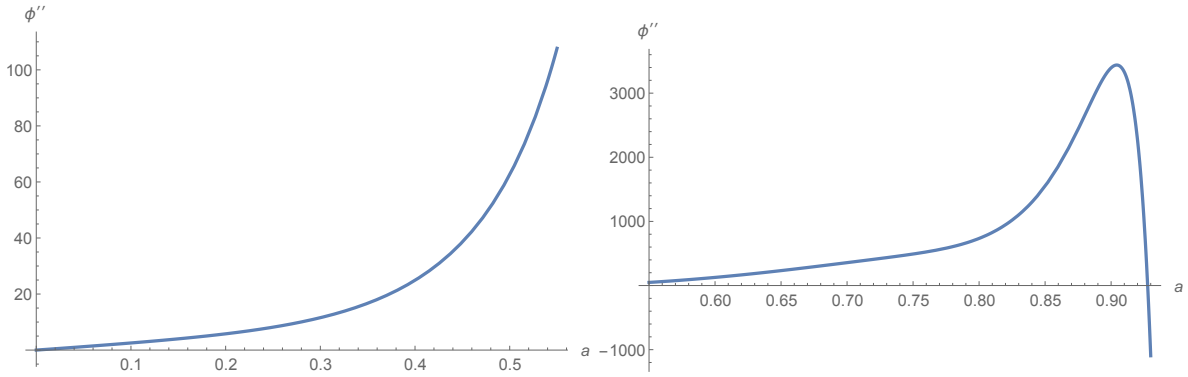

Figure 4. $\phi''(a)$.

For coercivity, we see that $\phi(a)$ is continuous for all positive values of a, $\phi(a) \to \infty$ as $a \to 0$ and when $a \to \infty$, $\phi(a)$ tends to ∞, which implies $\phi(a)$ is coercive. Hence, $\phi(a)$ attains $\inf_{(a)>0}\{\phi(a)\}$ at unique positive (a_0) and satisfies $\phi'(a_0) = 0$. □

4. Some numerical examples

As far as we know, star systems can configure in many forms: single stars, binary stars, triple stars, and even multiple-star systems. Astronomers currently estimate that up to 85 percent of stars may be in binary stars. Latest investigations have shown that the four-star system (especially two binary, which usually consists of two pairs of twin stars slowly circling each other at great distances) is itself more common than previously believed (e.g., Capella, 4 Centauri, Mizar, 30 Ari, Kepler-64b, Kepler-1652, HD98800, etc.).

Usually, the orbits of stars conserve information about the formation processes of the multiple star systems, and exploring dynamically their motion helps us to understand the evolution of stars. Accordingly, special types of the four-body problem investigated analytically and numerically can provide a better understanding of the dynamical behavior of quadruple stellar systems.

We take into consideration the given isosceles trapezoidal central configurations presented in Section 2.

Let us consider four point masses $m_0 = m_1 = 1, m_2 = m_3 = m$ on the vertices of a trapezoid as introduced in Section 2. Using position coordinates from Section 2 we obtain the following reduced Hamiltonian:

$$\begin{aligned} H &= \sum_{i=1}^{4} \frac{p_i^2}{2m_{i-1}} - \frac{m_0 m_1}{r_{12}} - \frac{m_0 m_2}{r_{13}} - \frac{m_0 m_3}{r_{14}} \\ &\quad - \frac{m_1 m_2}{r_{23}} - \frac{m_1 m_3}{r_{24}} - \frac{m_2 m_3}{r_{34}}, \end{aligned} \tag{4.1}$$

where

$$\begin{aligned} r_{12}^2 &= 1 + q_1^2, \quad r_{13}^2 = \left(\frac{a+1}{2}\right)^2 + (q_3 - q_1)^2, \\ r_{14}^2 &= \left(\frac{1-a}{2}\right)^2 + (\gamma - q_1)^2, \; r_{23}^2 = \left(\frac{a-1}{2}\right)^2 + q_3^2, \\ r_{24}^2 &= \left(\frac{a+1}{2}\right)^2 + \gamma^2, \quad r_{34}^2 = a^2 + (\gamma - q_3)^2, \end{aligned}$$

r_{ij}, $i = \overline{1,4}$, $i \neq j$, describes the position of the body P_i with respect to the body P_j, and q_i, p_i, $i = \overline{1,4}$ are the generalized coordinates and momenta (for simplicity we take the gravitational constant equal to 1).

The time evolution of the system is uniquely defined by Hamilton's equations:

$$\begin{aligned} \frac{dq}{dt} &= \frac{\partial H}{\partial p}, \\ \frac{dp}{dt} &= -\frac{\partial H}{\partial q}, \end{aligned} \tag{4.2}$$

where $H = H(q, p, t)$ is the Hamiltonian, which corresponds to the total energy of the system.

There are different behaviours for the solutions of Hamilton's equations. These flows of the vector fields can be drawn on a phase portrait. A very useful tool to understand these behaviours is the Poincaré map, which gives us a different way of analyzing the data.

We know that the Poincaré map is the intersection of a periodic orbit in the state space of a continuous dynamical system with a certain lower dimensional subspace, called the Poincaré section or surface of section, transversal to the flow of the system. It is a discrete dynamical system that is one dimension smaller than the original continuous periodic dynamical system. Therefore, the Poincaré section can be helpful to understand the behaviour of a dynamical system, and we use it for analyzing the reduced Hamiltonian system (4.2) to study the stability of periodic orbits.

For the investigation of the reduced Hamiltonian equations of motion (4.2), we have selected several examples of trapezoidal four-body problems. We tested two cases with different masses: $m < 1$ and $m > 1$. In both cases the Hamiltonian depends on the values a, b. In this direction, we chose three examples: $a < b$, $b < a$ and $a = b$. In these six situations we studied the quasiperiodic orbits implemented using the Poincaré surface of section technique by selecting the phase element $p_1 = 0$ [14, 15].

The structure of the whole center manifold can be better visualized by coloring the neighboring quasiperiodic trajectories and islands, which are shown in the following figures. The exterior curve in each plot is an orbit of the energy level corresponding to the plot. Inside the region, bounded by the exterior curve, chaotic scattering appears with some quasiperiodic orbits and chains of islands.

In the first example, with $a < b$, we have $a = 0.5$, $b = 1.5$, $m < 1$, $h \in \{-5.32, ..., -5.16\}$. We can distinguish three parts: the inner, the middle and the outer (Figure 5). At the $h = -5.32$ energy level the inner part is empty, the outer part is close to instability, and the middle part contains many invariant curves. At $h = -5.26$, -5.18 and -5.16, in the inner part appears a chaotic part of the "bell tilted to the left" form with some horseshoe periodic orbits. Moving outwards, the inner part break up and chains of islands in a chaotic band evolve in their place. Increasing the values of the energy, the outer part expands, grow up, and then loses its shape.

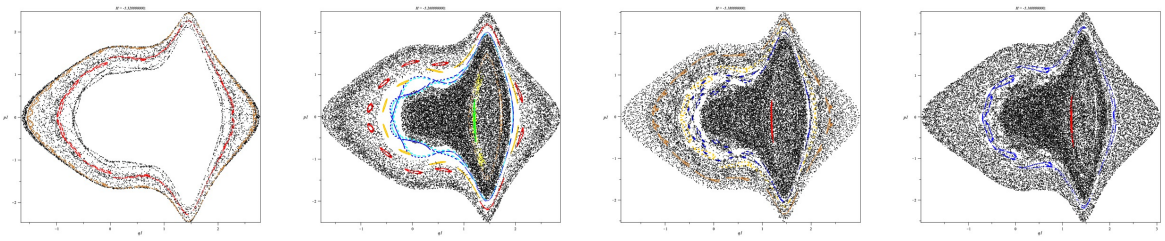

Figure 5. Examples of Poincaré surface of sections in case $a < b$ and $m < 1$ for possible energy levels interval {-5.32...-5.16}.

.

The second example, with $a < b$ has $a = 2.5$, $b = 5$, $m < 1$, $h \in \{-2.44, ..., -2.18\}$ (see Figure 6), and is a very interesting case. As the energy increases two horizontal lobes around two fixed points evolve in two vertical chaotic symbiotical parts. It seems to be a flow of material between two-part, as at the phenomenon possible between the binary stars. The initial "two horizontal lobes" domain is small, but as the energy increases, the initial domain expands in a more than six times larger area. The structure of the left initial part seems to evolve from the quasiperiodic trajectories through horseshoe orbits in a chaotic scattering and merge together with the right part. Increasing the values of the energy, the particles finally escape the system.

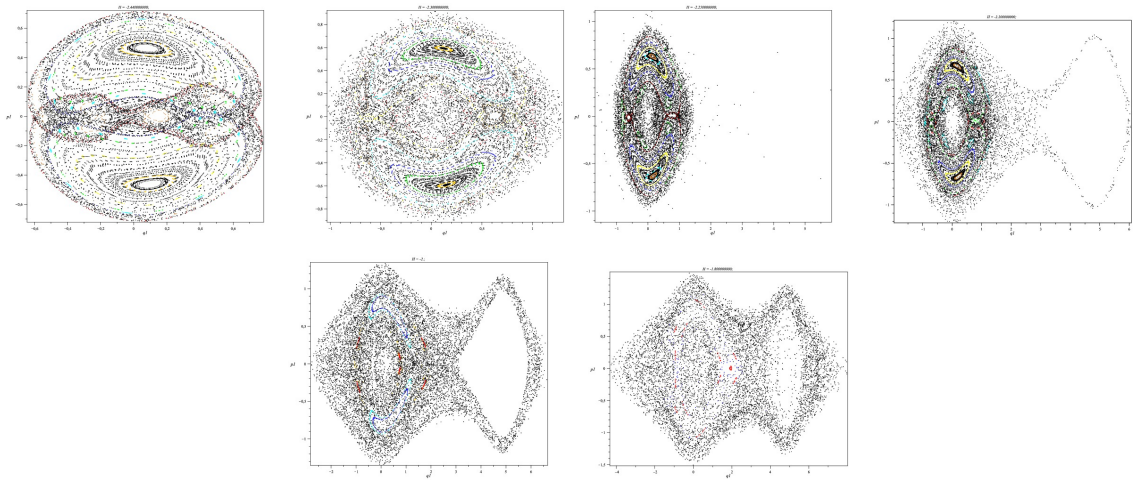

Figure 6. Examples of Poincaré surface of sections in case $a < b$ and $m < 1$ for possible energy levels interval $\{-2.44... - 2.18\}$.

The third example, when $a > b$, $a = 1.5$, $b = 0.5$, $m < 1$, $h \in \{-5.86, ..., -5\}$ (see Figure 7), shows invariant curves around the central stable fixed point. The closed curves break up and chains of islands and chaotic bands evolve in their places. At some energy levels, the inside of the "rhombus" form advances in an empty region. Farther out with increasing h, scattered points appear at the exterior orbit, representing escaping particles, and the inside part becomes empty.

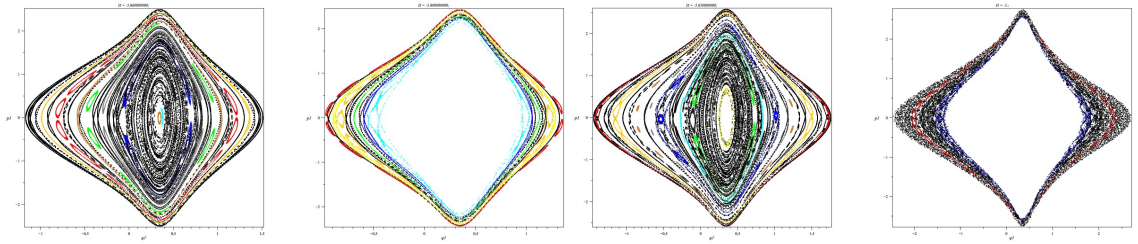

Figure 7. Examples of Poincaré surface of sections in case $a > b$ and $m < 1$ for possible energy levels interval $\{-5.86... - 5\}$.

The fourth example, when $a = b = 2$, $m < 1$, $h \in \{-3.6, ..., -3.2\}$ (see Figure 8), has a right fixed point with empty domain around, and we can observe the appearance of islands and of a chaotic region. With Increasing value of the energy, the surface of section increases in area, and the islands are replaced by chaos.

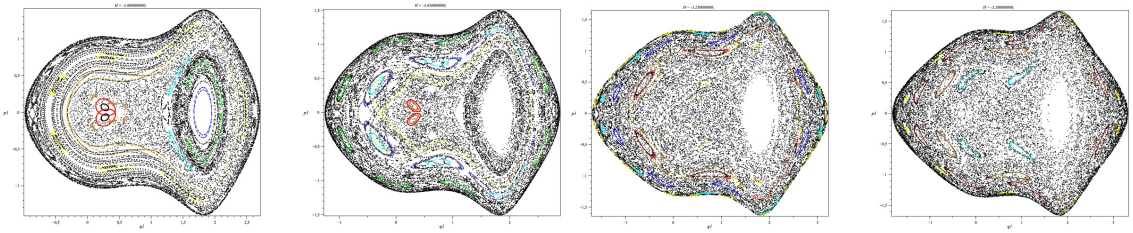

Figure 8. Examples of Poincaré surface of sections in case $a = b = 2$ and $m < 1$ for possible energy levels interval $\{-3.6... - 3\}$.

In the fifth example, when $a < b$, $a = 0.5$, $b = 1.2$, $m > 1$, $h \in \{-9.7, ..., -8.7\}$ (see Figure 9), at the energy value $h = -9.7$, quasi-periodic orbits appear with a chain of islands. A small increase in the value of energy makes that the middle part becomes chaotic, and around the right side fixed point emerge quasi-periodic and horseshoe orbits. Increasing the value of the energy, the surface of section increases in area, and the whole structure is replaced by chaos.

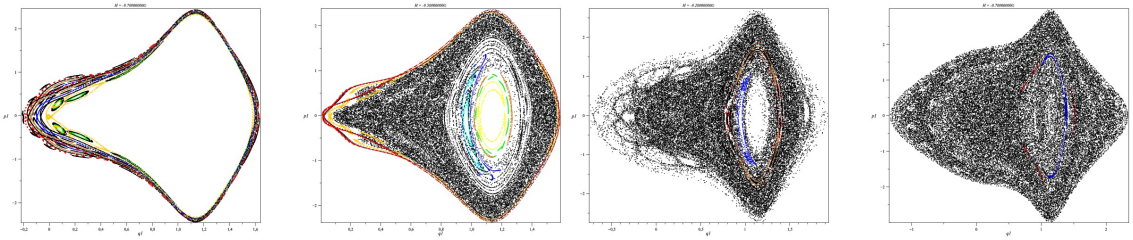

Figure 9. Examples of Poincaré surface of sections in case $a < b$ and $m > 1$ for possible energy levels interval $\{-9.7... - 8.7\}$.

In the sixth example, when $a < b$, $a = 2.5$, $b = 5$, $m > 1$, $h \in \{-3.41, ..., -3.12\}$ (see Figure 10), we can see a similar "material flow" effect as in the $m < 1$ case, but now with existing right side fixed point. In this situation also one can observe that in the structure of the left hemisphere, as the value of the energy increases, the quasi-periodic orbits evolve in a chaotic background. The right hemisphere becomes empty inside and by increasing the energy, this part also progresses in to chaos.

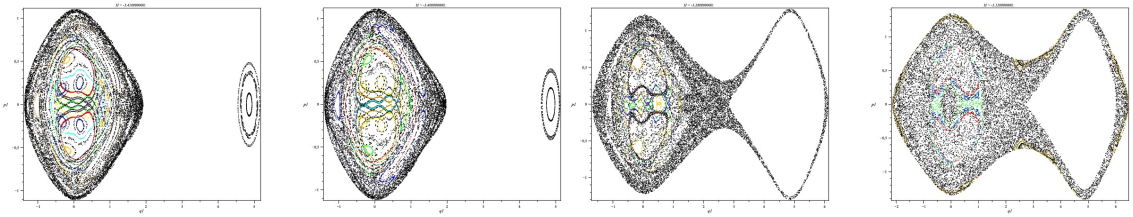

Figure 10. Examples of Poincaré surface of sections in case $a < b$ and $m > 1$ for possible energy levels interval $\{-3.41... - 3\}$.

The seventh example, ($a > b$, $a = 1.5$, $b = 0.5$, $m > 1$, $h \in \{-10.9, ..., -8.5\}$; see Figure 11) is similar to the $m < 1$ case in structure and topology. The obvious difference is around the central fixed point. In this case, the empty space around this central point is bigger than in the case $m < 1$.

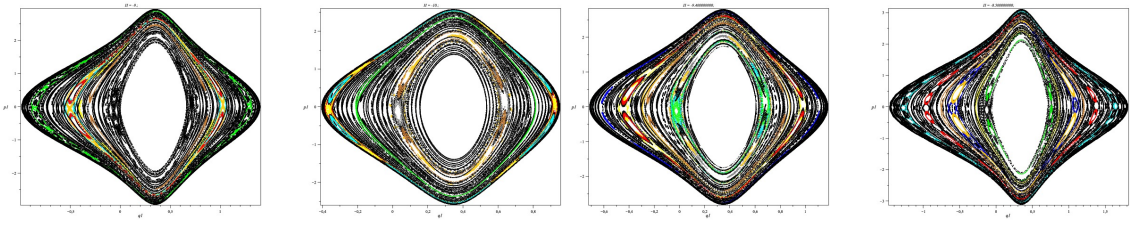

Figure 11. Examples of Poincaré surface of sections in case $a > b$ and $m > 1$ for possible energy levels interval $\{-10.9... - 8.5\}$.

In the eighth example, ($a = b = 2$, $m > 1$, $h \in \{-5.57, ..., -4\}$; see Figure 12), when the value of the energy increases, the exterior orbits and the left-center part show quasi-periodic trajectories,while the right and the inner part around the right fixed point have an empty structure until in the inner part appear chaotic behavior appears and the exterior part of the surface of section is deformed.

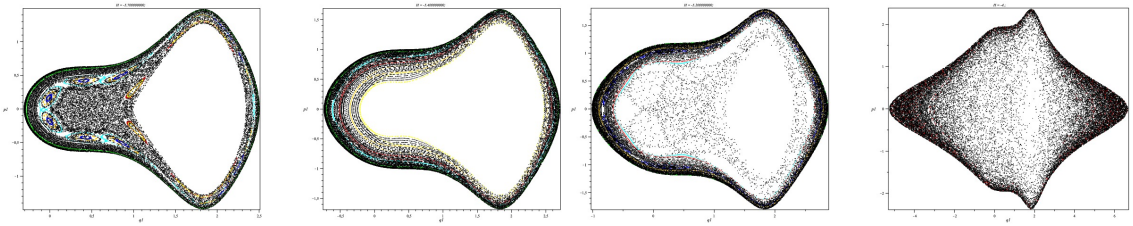

Figure 12. Examples of Poincaré surface of sections in case $a = b$ and $m > 1$ for possible energy levels interval $\{-5.7... - 4\}$.

5. Conclusions

In these examples, one can observe widespread chaotic regions, and the fact that some regular trajectories still survive. A comparison between the cases when $m < 1$ and $m > 1$ indicates a similar topology of the surface of structure (for a small variation of the value of the masses), and the interior structure depend strongly on an initial conditions.

The isosceles trapezoidal four-body problem, as a special case of the trapezoidal problem of four bodies, shows the main characteristic properties of such dynamical problems, for example the periodic and escape orbits.

Use of AI tools declaration

The authors declare they have not used Artificial Intelligence (AI) tools in the creation of this article.

Acknowledgments

I. Szücs-Csillik is partially supported by a grant from the Ministry of Research and Innovation, CNCS–UEFISCDI, project number PN-III-P2-2.1-SOL-2021-2-0192, within PNCDI III, and a grant from European Commission, Research Executive Agency, Specific Agreement Number 952852-2-3SST2018-20.

Conflict of interest

The authors declare that they have no conflicts of interest.

References

1. W. B. Gordon, A minimizing property of Keplerian orbits, *Amer. J. Math.*, **99** (1977), 961–971.
2. S. Q. Zhang, Q. Zhou, A minimizing property of eulerian solutions, *Celest. Mech. Dyn. Astron.*, **90** (2004), 239–243. https://doi.org/10.1007/s10569-004-0418-4
3. S. Q. Zhang, Q. Zhou, A minimizing property of Lagrangian solutions, *Acta Math. Sinica*, **17** (2001), 497–500. https://doi.org/10.1007/s101140100124
4. A. Mansur, Instability of periodic orbits of some rhombus and parallelogram four body problems, 2012.
5. A. Mansur, D. Offin, A minimizing property of homographic solutions, *Acta Math. Sin. English Ser.*, **30** (2014), 353–360. https://doi.org/10.1007/s10114-013-1299-9
6. A. Mansur, The Maslov index of periodic orbits in the linearized rhombus four body problem, *Int. J. Mech. Eng. Technol.*, **8** (2017), 1121–1136.
7. A. Mansur, D. Offin, M. Lewis, Instability for a family of homographic periodic solutions in the parallelogram four body problem, *Qual. Theory Dyn. Syst.* **16** (2017), 671–688. https://doi.org/10.1007/s12346-017-0232-5
8. K. C. Chen, Action minimizing orbits in the parallelogram four body problem with equal masses, *Arch. Rational Mech. Anal.*, **158** (2001), 293–318. https://doi.org/10.1007/s002050100146
9. A. Mansur, D. Offin, A. Arsie, Extensions to Chen's minimizing equal mass parallelogram solutions, *Taiwan. J. Math.*, **21** (2017), 1437–1453. https://doi.org/10.11650/tjm/171003
10. M. Santoprete, On the uniqueness of trapezoidal four-body central configurations, *Nonlinearity*, **34** (2021), 424–437. https://doi.org/10.1088/1361-6544/abbe61
11. M. Shoaib, Central configurations in the trapezoidal four-body problems, *Appl. Math. Sci.*, **9** (2015), 1971–1979. https://doi.org/10.12988/ams.2015.5173
12. M. Shoaib, A. R. Kashif, A. Sivasankaran, Planar central configurations of symmetric five-body problems with two pairs of equal masses, *Adv. Astron.*, **2016** (2016), 9897681. https://doi.org/10.1155/2016/9897681
13. M. Shoaib, A. R. Kashif, I. Szücs-Csillik, On the planar central configurations of rhomboidal and triangular four- and five-body problems, *Astrophys. Space Sci.*, **362** (2017), 182. https://doi.org/10.1007/s10509-017-3161-5
14. E. S. Cheb-Terrab, H. P. de Oliveira, Poincaré sections of Hamiltonian systems, *Comput. Phys. Commun.*, **95** (1996), 171–189. https://doi.org/10.1016/0010-4655(96)00032-X
15. I. Szücs-Csillik, The lie integrator and the Hénon-Heiles system, *Rom. Astron. J.*, **20** (2010), 49–66.

Supplementary

$$\begin{aligned}\eta'(a) &= \frac{2r_3(a)^2m'(a)}{r_1(a)^2} - \frac{4m(a)r_3(a)^2r_1'(a)}{r_1(a)^3} \\ &+ \frac{4m(a)r_3(a)r_3'(a)}{r_1(a)^2}.\end{aligned}$$

$$\begin{aligned}\eta''(a) &= \frac{2r_3(a)^2m''(a)}{r_1(a)^2} - \frac{8r_3(a)^2m'(a)r_1'(a)}{r_1(a)^3} \\ &+\frac{8r_3(a)m'(a)r_3'(a)}{r_1(a)^2} + \frac{12m(a)r_3(a)^2r_1'^2}{r_1(a)^4} \\ &-\frac{16m(a)r_3(a)r_1'(a)r_3'(a)}{r_1(a)^3} + \frac{4m(a)r_3'^2}{r_1(a)^2} \\ &-\frac{4m(a)r_3(a)^2r_1''(a)}{r_1(a)^3} + \frac{4m(a)r_3(a)r_3''(a)}{r_1(a)^2}.\end{aligned}$$

$$\begin{aligned}\xi'(a) &= m(a)r_1(a)(-\frac{m(a)}{a^2} - \frac{2f'(a)}{f(a)^2} - \frac{2f(a)f'(a)+1}{(f(a)^2+a)^{3/2}} \\ &+\frac{m'(a)}{a}) \\ &+r_1(a)(\frac{2}{f(a)} + \frac{2}{\sqrt{f(a)^2+a}} + \frac{m(a)}{a})m'(a) \\ &+m(a)(\frac{2}{f(a)} + \frac{2}{\sqrt{f(a)^2+a}} + \frac{m(a)}{a})r_1'(a) + r_1'(a).\end{aligned}$$

$$\begin{aligned}\xi''(a) &= 2r_1(a)m'(a)(-\frac{m(a)}{a^2} - \frac{2f'(a)}{f(a)^2} - \frac{2f(a)f'(a)+1}{(f(a)^2+a)^{3/2}} + \frac{m'(a)}{a}) \\ &+2m(a)r_1'(a)(-\frac{m(a)}{a^2} - \frac{2f'(a)}{f(a)^2} - \frac{2f(a)f'(a)+1}{(f(a)^2+a)^{3/2}} + \frac{m'(a)}{a}) \\ &+m(a)r_1(a)(\frac{2m(a)}{a^3} - \frac{2m'(a)}{a^2} - \frac{2f''(a)}{f(a)^2} + \frac{4f'^2}{f(a)^3} \\ &+\frac{3(2f(a)f'(a)+1)^2}{2(f(a)^2+a)^{5/2}} - \frac{2f(a)f''(a)+2f'^2}{(f(a)^2+a)^{3/2}} + \frac{m''(a)}{a}) \\ &+r_1(a)(\frac{2}{f(a)} + \frac{2}{\sqrt{f(a)^2+a}} + \frac{m(a)}{a})m''(a) \\ &+2(\frac{2}{f(a)} + \frac{2}{\sqrt{f(a)^2+a}} + \frac{m(a)}{a})m'(a)r_1'(a) \\ &+m(a)(\frac{2}{f(a)} + \frac{2}{\sqrt{f(a)^2+a}} + \frac{m(a)}{a})r_1''(a) + r_1''(a).\end{aligned}$$

$$f'(a) = \begin{cases} f_1'(a) \text{ when } a \in (0, 0.55) \\ f_2'(a) \text{ when } a \in (0.55, 1), \end{cases}$$

$$\begin{aligned} f_1'(a) &= 0.366506a^2 + 0.126123a - 0.235388, \\ f_1''(a) &= 0.733011a + 0.126123, \\ f_2'(a) &= 671.032a^5 - 2510.18a^4 + 3723.63a^3 \\ &\quad -2736.2a^2 + 996.52a - 144.032, \\ f_2''(a) &= 3355.16a^4 - 10040.7a^3 + 11170.9a^2 \\ &\quad -5472.4a + 996.52. \end{aligned}$$

AIMS Press